WELDING RESEARCH

SUPPLEMENT TO THE WELDING JOURNAL, MARCH, 1985

Sponsored by the American Welding Society and the Welding Research Council
TECHNICAL PAPERS EDITOR: T.P. SCHOONMAKER

Influence of Microstructure on Mechanical Properties of Two Single-Bead Ferritic Weld Metals

Submicron differences for each constituent in ferritic weld metals have an effect on weld metal toughness, and a "fracture sensitivity" measure indicates a different resistance to cleavage for each constituent

BY M. A. MUNNIG SCHMIDT-VAN DER BURG, S. HOEKSTRA, AND G. DEN OUDEN

ABSTRACT. The microstructures and mechanical properties of two single-bead ferritic weld metals are compared in the as-welded and artificially aged condition. The observed notch toughness behavior of both weld metals can only be understood, if differences between the principal microstructural constituents on a submicron scale are taken into account. These differences appear to be responsible for an increase in hardness and strength, offsetting the beneficial effects of more acicular ferrite and a finer microsctructure.

The individual constituents can be characterized by microhardness and crack propagation path measurements. The mutual differences are expressed in terms of a fracture sensitivity parameter, indicating a different resistance to cleavage for each microstructural constituent. It is emphasized that transmission electron microscopy, in combination with microanalytical techniques, is needed to reveal further details.

Introduction

There is a growing interest in the relationship between microstructure and mechanical properties with a view to the development of weld metals with optimum strength and toughness (Ref. 1). This interest is not surprising, because it is very attractive to be able to understand the mechanical properties of weld metal from the observed microstructure.

In the case of low alloyed ferritic weld metal, the literature indicates that a low ductile-brittle transition temperature, *i.e.*, a high resistance to cleavage, will occur when the proportion of acicular ferrite is high and that of grain boundary ferrite and ferrite with aligned M-A-C (Martensite-Austenite-Carbide) correspondingly low (Ref. 2). On the other hand, an increase in the amount of acicular ferrite in the microstructure is not always beneficial to weld metal toughness, if the deposit yield strength increases too much as a result of phenomena-like solid solution hardening or precipitation hardening. The net effect of these factors may even be negative, and so toughness decreases (Refs. 3,4).

As is known, the microstructure is determined by the thermal history and the chemical composition of the weld metal (Refs. 5,6). Cooling after solidification can be characterized by the austenization and transformation conditions, the effect of which is clear on the basis of Continuous Cooling and Transformation (CCT) diagrams. The influence of chemical composition is expressed by a change in shape and a shift of the CCT diagram to shorter or longer times. In this respect, the interaction of the major alloying elements is especially important in terms of their effect on the development of acicular ferrite.

Investigation Objectives

The aim of the present investigation was to characterize the microstructural constituents of low alloyed ferritic weld metal and to understand their influence on the resistance to cleavage fracture. For a better understanding of the relationship between microstructure and mechanical properties, it seemed appropriate to study single-bead weld metal in

M. A. MUNNIG SCHMIDT-VAN DER BURG and S. HOEKSTRA are with Philips Research Laboratories, Eindhoven, and G. DEN OUDEN is with the Delft University of Technology, Delft, The Netherlands.

the as-welded condition. However, multipass weld deposits are of far more practical importance but are subject to dynamic strain aging, due to thermal cycles and plastic deformation of subsequent layers of weld metal.

As is known, dynamic strain aging can be detrimental to the notch toughness of, in particular, the root weld pass of the weld deposit (Refs. 7,8). Therefore, the two single-bead ferritic weld metals used in this investigation were studied in the as-welded condition and after artificial aging consisting of a deformation of 6% followed by a heat treatment of 30 minutes (min) at 250°C (482°F). Such a simulation is considered to be a reasonable approximation of the processes occurring in the root weld pass of a multipass weld deposit (Refs. 7-9).

In the present study, quantitative metallography with the aid of light microscopy and scanning electron microscopy was used in characterizing the microstructures of both weld metals. These results were completed by Charpy V-notch, tensile, and overall hardness data. The individual microstructural constituents were characterized by microhardness and crack propagation path measurements.

Experimental Procedure

The two weld metals studied in this investigation were obtained by shielded metal arc welding (SMAW) using two types of low hydrogen electrodes with different coating compositions according to AWS standards E7016-C1L and E8018-C1; they are indicated as weld metal A and B, respectively. The welding conditions are presented in Table 1 and are the same for both weld metals.

The welds were deposited as single beads in 20 mm (0.79 in.) thick base plates supported by a backing strip as shown schematically in Fig. 1. To prevent dilution with the base metal as much as possible, all plates were buttered with the same electrode material. The chemical composition of the weld metals thus obtained is shown in Table 2.

Table 1—Welding Conditions

Welding current, A	~230
Arc voltage, V	~27.5
Heat input, kJ/mm	2.6
Travel speed, mm/s (ipm)	2.4 (5.7)
Electrode diameter, mm (in.)	5 (0.2)
Electrode length, mm (in.)	450 (17.7)

From these welds a number of Charpy V-notch impact specimens were cut out mechanically as indicated in Fig. 1A. The limited height of the deposits made it necessary to use subsize Charpy specimens with dimensions of 3 × 10 × 55 mm (0.12 × 0.39 × 2.17 in.). Specimens used for artificial aging experiments, however, had dimensions of 3.3 × 11.5 × 55 mm (0.13 × 0.45 × 2.17 in.) and were then 6% deformed by a compression test parallel to the direction of welding as described elsewhere (Ref. 10). Before these specimens were machined to 3 × 10 × 55 mm (0.12 × 0.39 × 2.17 in.), they were heat treated for 30 min at 250°C (482°F). In all cases the notch of the Charpy specimens was located at the center of the weld—Fig. 1A.

Table 2—Chemical Compositions of Weld Metals A and B, Wt-%

	Weld metal	
	A	B
C	0.064	0.061
Mn	0.58	1.08
Si	0.20	0.15
Ni	2.50	2.50
P	0.012	0.011
S	0.008	0.006
Ti	0.011	0.005
Cr	0.05	0.04
Cu	0.02	0.02
V	0.007	0.009
Al	0.0005	0.0005
B	0.0001	0.0008
O	0.026	0.036
N	0.010	0.016

All-weld-metal tensile specimens, with a diameter of 4 mm (0.16 in.) and a gauge length of 40 mm (1.57 in.) were taken from the weld bead in the longitudinal direction as shown in Fig. 1B. Artificial aging of these specimens consisted of a plastic deformation of 6% in a tensile testing machine followed by the same heat treatment as described above.

Specimens for scanning electron microscopy were abraded on water-cooled silicon carbide (SiC) paper followed by electrolytic polishing for 8 seconds(s) in a solution of A-2 (Struers) at a voltage of 55 V and flow rate 3 (Struers Polectrol). In the case of light microscopy this procedure was followed by chemical etching of the specimens in 2% nital for 15 s. The plane of viewing was parallel to the surface of the base metal and located in the center of the weld metal.

The same specimens were used for Vickers hardness measurements with the aid of a Leitz Durimet microhardness tester. The overall hardness was obtained with a load of 1000 g (2.2 lb), while the microhardness of the individual microstructural constituents was determined with a load of 25 g (0.88 oz).

A quantitative description of the secondary microstructure was obtained by making use of a Swift Point Counter model F (with a step-size of 5 μm (0.0002 in.) and 1000 counts for each weld metal) attached to a Leitz Orthoplan light microscope at magnifications of 200 and 500 times. This description was based on the nomenclature proposed by Abson and Dolby (Ref. 11) for as-deposited ferritic weld metal microstructures.

A Philips 505 scanning electron microscope was used to examine the fracture surface of broken impact specimens and to analyze volume fraction and size distribution of non-metallic inclusions on polished surfaces. Analytical electron micros-

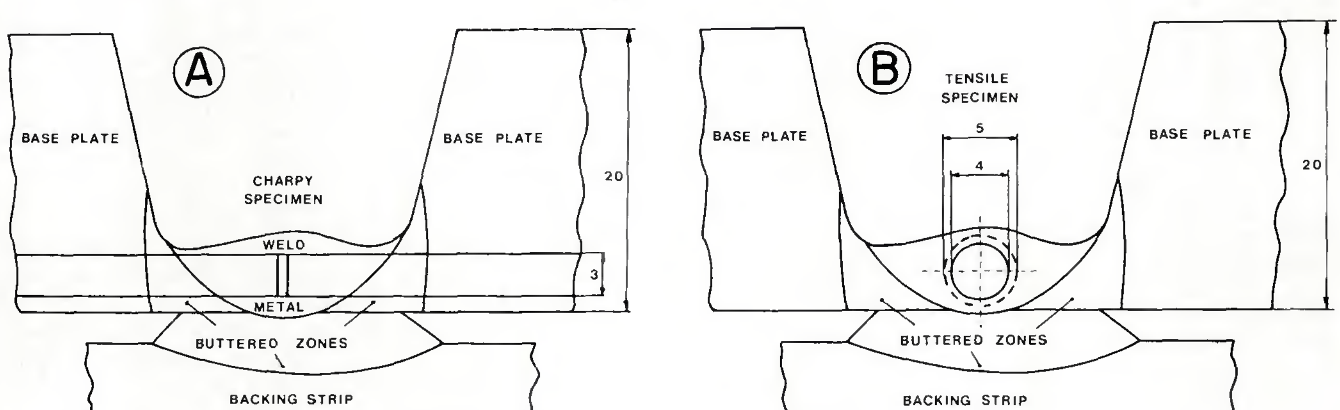

Fig. 1—Schematic representation of the weld geometry and the location of the Charpy and tensile specimens

copy (EDX) and electron microprobe (WDX) measurements were carried out for qualitative microanalysis of the inclusions and the matrix of both weld metals.

Results

Microstructural Features

Grain Size. The principal constituents of the secondary microstructure, which had to be considered for both weld metals, are grain boundary ferrite (GF), ferrite with aligned M-A-C (AC), and acicular ferrite (AF). Examples of the secondary microstructure of weld metals A and B are shown in Figs. 2 and 3, respectively.

It was found that the grain size of the prior austenite (primary microstructure) is about the same for both weld metals. However, the grain size of the individual constituents of the secondary microstructure is quite different in the two weld metals as can be seen from Figs. 2 and 3. The grain size of these constituents was measured with the aid of the linear intercept method at a magnification of ×200 for grain boundary ferrite and ferrite with aligned M-A-C and at a magnification of ×500 for acicular ferrite; the results are shown in Table 3. In the case of ferrite with aligned M-A-C the grain size was characterized by the mean length and width of the individual plates with an aspect ratio of about 10 for both weld metals. If ferrite with aligned M-A-C is considered as a packet-like structure, because of the low angle boundaries between the individual plates, then it is clear that this microstructural constituent has the largest grain size followed by grain boundary ferrite and acicular ferrite, respectively.

From Table 3 it can also be seen that the microstructural constituents of weld metal B are smaller in size than those of weld metal A. Apart from grain size, no differences could be observed between corresponding constituents in both weld metals based on light microscopic investigations.

Quantitative Description of the Microstructure. The point counting results (step-size 5 μm, *i.e.*, 0.0002 in.) of the microstructural constituents are shown in Table 4. These results indicate that weld metal B contains less grain boundary ferrite and correspondingly more acicular ferrite than weld metal A, while the proportion of ferrite with aligned M-A-C is roughly the same for both weld metals.

Light microscopy of both weld metals did not reveal any difference between the as-welded and artificially aged condition. The same result was found when scanning electron microscopy was used to study fracture surfaces of broken Charpy impact specimens.

Size distributions of non-metallic inclusions on polished surfaces were measured with the aid of scanning electron microscopy at a magnification of ×2500. These distributions were obtained by counting the number of inclusions with a specific diameter on ten scanning electron micrographs representing a total area of 0.016 mm^2 (2.5 × 10^{-5} in.).

The results of these measurements are shown in Fig. 4. It can be seen that the size distribution is roughly the same for both weld metals, although the average diameter of the inclusions in weld metal A is somewhat higher (0.50 μm, *i.e.*, 2 × 10^{-6} in.) than that in weld metal B (0.45 μm, *i.e.*, 1.8 × 10^{-6} in). Furthermore it appears that the inclusion volume fractions are similar at about 0.27%. However, the number of inclusions in weld metal B is clearly more than that in weld metal A. This agrees with the observation that the mean dimple size of ductile fractured Charpy impact specimens is smaller for weld metal B than for weld metal A.

Qualitative Microanalysis. The matrix composition of both weld metals can be characterized by Fe, Ni, Mn and Si with weld metal B containing more Mn than weld metal A. In both cases the Ti content of the matrix is lower than the detection limit. The inclusions are mainly composed of Mn, Si and Ti, while in a few cases only Mn, or Mn and S, or Mn

Table 4—Proportion of the Principal Microstructural Constituents in Weld Metals A and B

Constituents	Proportion of constituents, %	
	A	B
GF	54.4	34.0
AC	18.2	16.3
AF	27.4	49.7

Table 3—Grain Size of the Principal Microstructural Constituents in Weld Metals A and B

Constituents	Grain size of constituents, μm	
	A	B
GF	34	20
AC(a)	127/12	85/9
AF	6	5

(a) For constituent AC, the mean length and width of the individual plates are given.

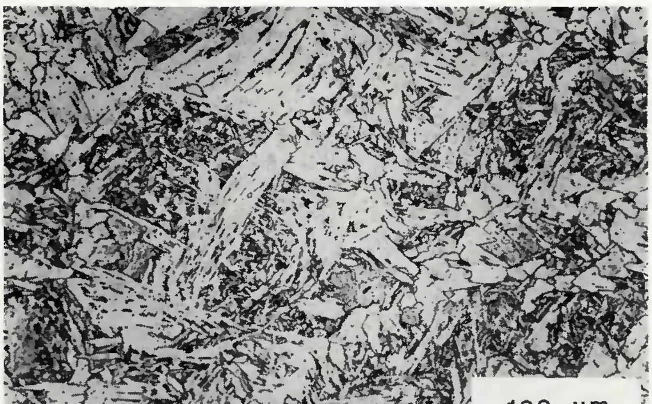

Fig. 2—Light optical micrograph of weld metal A. Etchant: 2% nital

Fig. 3—Light optical micrograph of weld metal B. Etchant: 2% nital

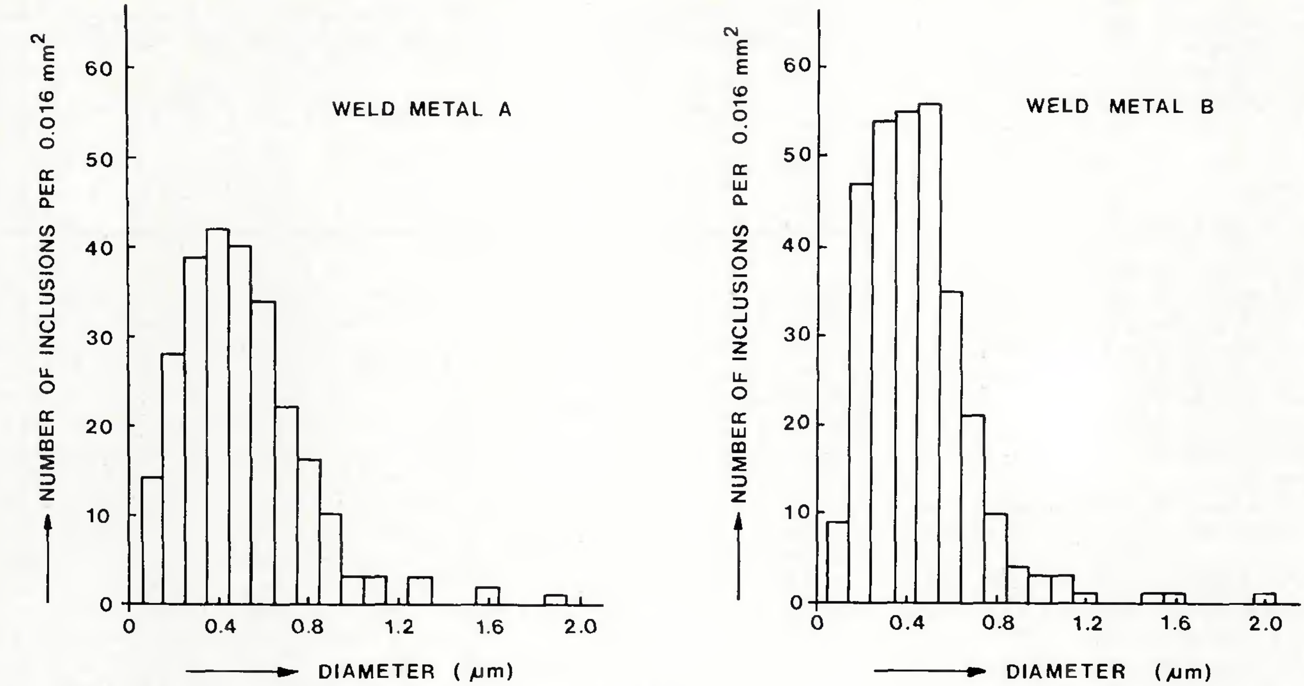

Fig. 4 — Size distribution of non-metallic inclusions in weld metals A and B

and Si was detected.

These compositions suggest the presence of oxides, sulphides and silicates. The inclusions of weld metal A have a higher Ti and Si content than those of weld metal B. In both weld metals, the inclusions show a higher Mn, Si and Ti content than the matrix. In other words, the inclusions and the matrix of weld metals A and B have a different Mn:Ti:Si ratio.

Mechanical Properties

Charpy V-Notch Toughness. The results of Charpy V-notch measurements are shown in Fig. 5. The ductile-brittle transition temperature (T_o) is derived from the average value between the lower and upper shelf energy. It can be seen that, in the as-welded condition, weld metal A has a better toughness behavior than weld metal B.

Upon artificial aging, however, the transition curve of weld metal A shows a

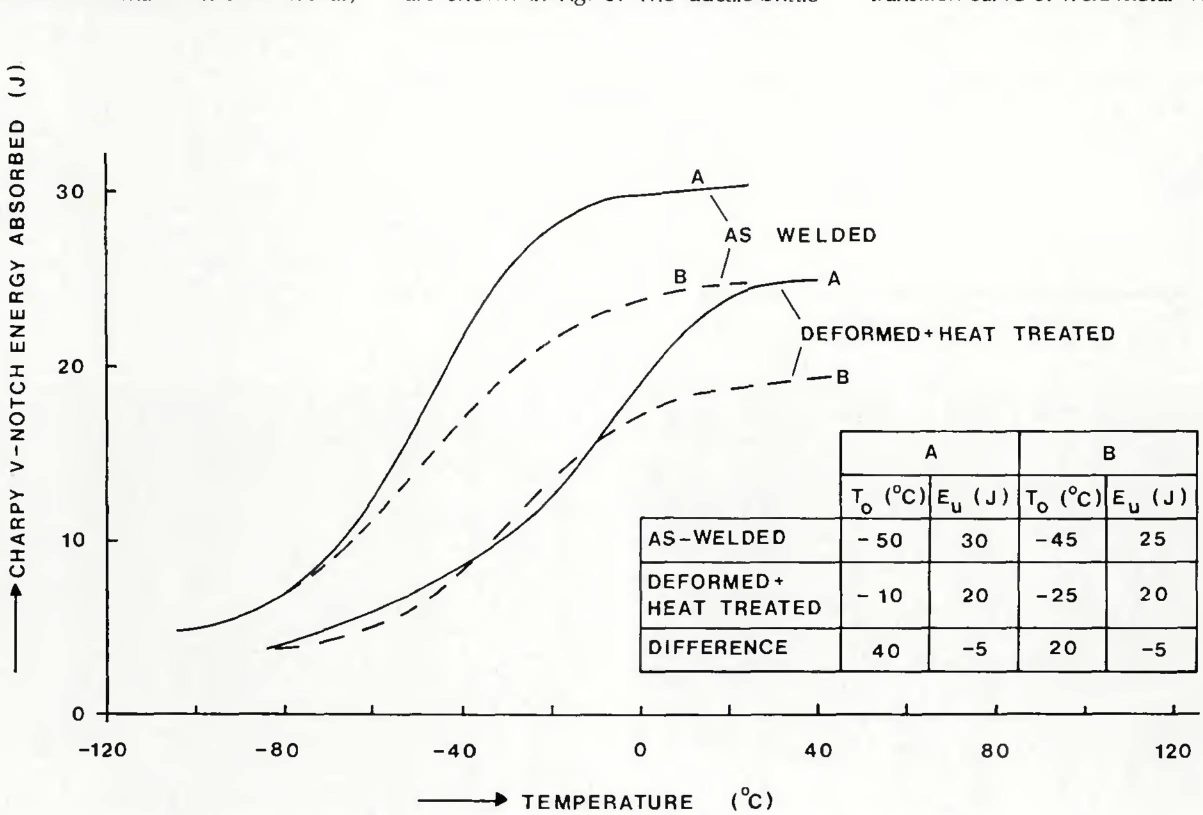

	A		B	
	T_o (°C)	E_u (J)	T_o (°C)	E_u (J)
AS-WELDED	-50	30	-45	25
DEFORMED+ HEAT TREATED	-10	20	-25	20
DIFFERENCE	40	-5	20	-5

Fig. 5 — Charpy V-notch transition curves of weld metals A and B in the as-welded and artificially aged condition

Table 5—Vickers Overall Hardness of Weld Metals A and B Measured With a Load of 1000 g (2.2 lb)

Weld metal	A	A → B	B
As-welded	175	+14%	199
	↓ +19%		↓ +19%
Deformed	208	+14%	237
	↓ +11%		↓ +11%
Deformed + heat treated	230	+14%	262

larger shift to higher temperatures than weld metal B. During this shift the upper shelf energies of both weld metals decrease by the same amount as shown in Fig. 5.

Hardness. The overall hardness of both weld metals was measured with a load of 1000 g (2.2 lb). It can be seen from Table 5 that in each of the three conditions the hardness of weld metal B is 14% higher than that of weld metal A (each value is the average of 12 measurements). Deforming the weld metal causes an increase in hardness of 19%, while a further increase of 11% is caused by the subsequent heat treatment of the aging process. In both cases the increase in hardness is the same for weld metal A and B.

The microhardness of the individual microstructural constituents of both weld metals was measured with a load of 25 g (0.055 lb). The results of these measurements are shown in Table 6, where each value is the average of 10 measurements. As can be seen, each constituent in weld metal B has a higher hardness than the corresponding constituent in weld metal A. This holds for each of the three conditions indicated in Table 6 where grain boundary ferrite reveals the lowest microhardness, followed by ferrite with aligned M-A-C, and acicular ferrite representing the highest microhardness.

Deforming the weld metal results in a different hardness increase for the three constituents. In both weld metals, grain boundary ferrite shows the largest increase, followed by ferrite with aligned M-A-C and acicular ferrite, respectively. The heat treatment of the artificial aging process, however, causes an extra increase in hardness, which is the same for the three constituents, *i.e.*, 12% in the case of weld metal A and about 9% in the case of weld metal B.

Strength. The results of measurements on all-weld-metal tensile specimens are shown in Table 7. It appears that in the as-welded and artificially aged condition, weld metal B has higher yield (σ_Y) and ultimate tensile (σ_{UTS}) strengths and a correspondingly lower elongation at fracture (ϵ_F) than weld metal A.

Upon artificial aging, the yield and tensile strengths increase and the total elongation at fracture decreases. These effects are more pronounced for weld metal B than for weld metal A. Note that, for both weld metals, the yield strength equals the tensile strength in the artificially aged condition due to the relatively high deformation of 6%.

Discussion

The microstructure of as-deposited ferritic weld metal is determined by its chemical composition and the cooling procedure during welding. The grain size of the primary microstructure and the cooling procedure are similar for both weld metals. For this reason, it is clear that the differences in the secondary microstructure can only be ascribed to differences in chemical composition.

These differences chiefly involve the Mn, Si, Ti, O and N content as shown in Table 2. The higher Mn content of weld metal B is responsible not only for the higher proportion of acicular ferrite at the expense of grain boundary ferrite, but also for a finer grain size of the secondary microstructure as described by Evans (Ref. 12) and Farrar and Watson (Ref. 13). Despite these positive effects, weld metal B does not show a better notch toughness behavior than weld metal A. Regarding the resistance to cleavage fracture, this discrepancy can only be understood in terms of differences on a submicron scale between corresponding constitu-

Table 6—Vickers Microhardness of the Principal Microstructural Constituents of Weld Metals A and B Measured With a Load of 25 g (0.9 oz)

	GF			AC			AF		
Weld metal	A	A → B	B	A	A → B	B	A	A → B	B
As-welded	176	+9%	191	202	+8%	219	222	+6%	236
	↓ +21%		↓ +28%	↓ +18%		↓ +16%	↓ +11%		↓ +15%
Deformed	213	+15%	244	238	+7%	254	247	+10%	272
	↓ +12%		↓ +9%	↓ +12%		↓ +9%	↓ +12%		↓ +10%
Deformed + heat treated	238	+12%	266	266	+4%	276	277	+8%	300

Table 7—Strength Data of Weld Metals A and B in the As-Welded and Artificially Aged Condition

	σ_Y N/mm^2			σ_{UTS} N/mm^2			ϵ_F, %		
Weld metal	A	A → B	B	A	A → B	B	A	A → B	B
As-welded	458	+5%	482	580	+11%	643	18	−17%	15
	↓ +40%		↓ +54%	↓ +11%		↓ +15%	↓ −39%		↓ −47%
Deformed + heat treated	641	+16%	741	641	+16%	741	11	−27%	8

ents offsetting the higher proportion of acicular ferrite and the finer grain size of weld metal B as discussed elsewhere in the paper.

Fracture in the ductile mode has been found to be principally controlled by the nucleation of microvoids at inclusions. From the literature it is known that fewer inclusions produce a larger dimple size on a ductile fracture surface due to the smaller number of inclusions available to initiate microvoid coalescence (Ref. 14). This leads to a higher upper shelf energy of the transition curve because a larger dimple size is associated with a higher energy absorption.

From Figs. 4 and 5 it can be seen that these findings correspond with our measurements, because the larger number of inclusions in weld metal B causes a lower upper shelf energy as compared with weld metal A. Obviously, the number of inclusions available to initiate microvoid coalescence is more important in influencing the upper shelf energy than its volume fraction, because this is similar for both weld metals despite the difference in O content (Ref. 15).

The microhardness measurements give a clear picture of the microstructural differences between the principal constituents of the secondary microstructure — Table 6. Grain boundary ferrite exhibits the lowest hardness because of its relatively large grain size and low level of internal stress associated with the highest transformation temperature of the decomposition products of austenite (Ref. 16).

Ferrite with aligned M-A-C is usually produced at lower temperatures than grain boundary ferrite. The higher hardness of this constituent is mainly caused by the martensite-austenite (M-A) or carbide (C) microphases between the narrow ferrite plates. Acicular ferrite is formed at temperatures lower than ferrite with aligned M-A-C, and mostly exists in the interior of the prior austenite grains. The small grain size, high dislocation density, and high angle grain boundaries are responsible for the higher hardness of acicular ferrite compared with the other two microstructural constituents (Ref. 17).

The differences in hardness, microstructure and proportion of the principal constituents are responsible for the different increases in microhardness upon plastic deformation, as shown in Table 6. In both weld metals grain boundary ferrite, for instance, reveals the largest increase in hardness because the plastic strain primarily concentrates into this comparatively weak constituent (Ref. 2). This effect is more pronounced as the proportion of grain boundary ferrite decreases — Table 4. Therefore, weld metal B shows a larger increase in hardness for grain boundary ferrite upon plastic deformation than weld metal A.

In comparing the overall hardness measurements (Table 5) with the microhardness measurements (Table 6), it should be noted that the observed differences are partly due to the difference in test weight (25 and 1000 g). For this reason, only the percentage differences in overall hardness and microhardness may be compared.

First of all, the increase in hardness upon artificial aging will be considered. As discussed before, plastic deformation causes different increases in microhardness for the individual constituents — Table 6. However, when these percentage increases are multiplied by the corresponding proportion of each constituent (Table 4), it is possible to obtain the increase in overall hardness, ΔH. In the case of weld metal B, for instance, this leads to:

$\Delta H = 28\% * 0.34 + 16\% * 0.163 + 15\% * 0.497 = 19.6\%$

As can be seen, this calculated increase in overall hardness shows a fair correspondence with the measured value given in Table 5; it appears that the same holds for weld metal A.

The heat treatment of the artificial aging process reveals the same increase in hardness for each of the three constituents, *i.e.*, 12% in the case of weld metal A and about 9% in the case of weld metal B — Table 6. Because of this, it is allowed to compare these hardness increases directly with the overall hardness increase of 11% — Table 5. It can be seen that in this case too, a fair correspondence exists between Tables 5 and 6. Note that the same hardness increase upon heat treatment suggests similar aging processes in the different constituents.

The last comparison that can be made concerns the percentage hardness differences between weld metals A and B with regard to the overall hardness and the microhardness. For that purpose, an overall hardness has to be calculated by multiplying the proportion of each microstructural constituent (Table 4) by its corresponding microhardness — Table 6. In the case of weld metal A in the as-welded condition, for instance, the following hardness is obtained:

$H = 0.544*176 + 0.182*202 + 0.274*222 = 193$

This procedure has been applied to both weld metals in each of the three conditions, and yields the data shown in Table 8. As can be seen, the percentage differences between weld metal A and weld metal B correspond fairly well with those given in Table 5. The same conclusion can be drawn for the percentage increase in hardness upon deforming and heat treating the specimens.

Note that a calculation of the overall hardness from the microhardness also shows why the percentage differences between both weld metals for each constituent (Table 6) may all be smaller than the corresponding difference in overall hardness — Table 5. This can be explained by the different proportions of the corresponding constituents in weld metals A and B.

It is clear that the higher strength (Table 7) and hardness of weld metal B is partly caused by the finer grain size of the constituents (Hall-Petch relation) and the presence of more acicular ferrite than in weld metal A. Because both microstructural features are, in general, also beneficial to toughness, it is not clear — at least from a light microscopic point of view — why the resistance to cleavage of weld metal B does not exceed that of weld metal A.

Since the corresponding constituents of both weld metals are similar in the light microscope (except grain size), it is assumed that phenomena on a submicron scale play an important role in relation to the observed toughness behavior, offsetting the higher proportion of acicular ferrite and the finer grain size of weld metal B. A first indication in this respect is based not only on the microhardness measurements but also on the varying influence of artificial aging on toughness, overall hardness, and strength, as described above. A second indication is the small difference in grain

Table 8—Overall Hardness Data of Weld Metals A and B Calculated From the Microhardness and the Proportion of Each Principal Microstructural Constituent

	Weld metal A		Weld metal B
As-welded	193	→ +13% →	218
	↓ +18%		↓ +19%
Deformed	227	→ +15% →	260
	↓ +12%		↓ +10%
Deformed + heat treated	254	→ +12% →	285

size between the acicular ferrite of weld metal A (6 μm, *i.e.,* 0.00024 in.) and that of weld metal B (5 μm, *i.e.,* 0.0002 in.), which cannot completely be responsible for the difference in microhardness.

In our case it is most likely that the higher Mn content in the matrix of weld metal B causes solid solution hardening and, therefore, an extra increase in strength and hardness. Apart from the properties of the constituents themselves, it is also important to consider their mutual interaction. The harder acicular ferrite, for instance, concentrates the strain into the softer constituents (Refs. 2,18). This effect is more pronounced as the proportion of acicular ferrite increases. The subjection of crack nucleation sites (like inclusions or brittle microphases at grain boundaries) to these increasing strains leads to fracture at an earlier stage, and therefore to a lower toughness (Refs. 19,20).

A further attempt was made to reveal the submicron differences between the principal constituents by investigating the polished cross-section of broken Charpy specimens (half the thickness of 3 mm, *i.e.,* 0.12 in.) whose brittle fracture surface was protected with a nickel layer. An example (weld metal A in the as-welded condition) is shown in Fig. 6.

The point counting results (step-size 5 μm, *i.e.,* 0.0002 in., magnification ×500) of the principal constituents along the crack propagation path compared with the bulk proportions of these constituents (see Table 4), are presented in Table 9. Dividing the proportions along the crack path by the corresponding bulk proportions leads to a fracture sensitivity measure for each microstructural constituent. This measure indicates that, in both weld metals, ferrite with aligned M-A-C is the most sensitive one to brittle fracture, followed by grain boundary ferrite and acicular ferrite, respectively. In other words, acicular ferrite reveals the highest resistance to cleavage. The sequence in fracture sensitivity of the three constituents corresponds to their decreasing grain size (Table 3), if ferrite with aligned M-A-C is considered as a packet-like structure.

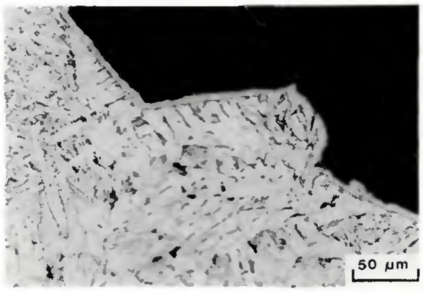

Fig. 6 — Cross-sectional profile of a crack propagation path through an as-welded Charpy V-notch specimen of weld metal A tested at −100°C, i.e., −148°F (also see Table 9)

According to Fig. 6, this assumption is justified, because in this micrograph the crack path runs through a number of parallel plates without changing its orientation. When the fracture sensitivity measures of the corresponding constituents are compared (Table 9), it appears that in weld metal B acicular ferrite and ferrite with aligned M-A-C have a lower resistance to cleavage than in weld metal A due to solid solution hardening of Mn. On the other hand, grain boundary ferrite has a somewhat higher resistance to cleavage in weld metal B than in weld metal A.

The higher resistance to cleavage can be explained by the much smaller grain size of this constituent in weld metal B (see Table 3), which obviously predominates detrimental effects like solid solution hardening. The fracture sensitivity condition indicates, however, that the improvement of grain boundary ferrite is negligibly small in comparison with the deterioration of the other two constituents. This means that the notch toughness behavior of both weld metals can be explained in terms of this parameter.

More information about the submicron differences between the constituents of both weld metals can be obtained with the aid of transmission electron microscopy (TEM) in combination with microanalytical techniques. However, an important prerequisite is the recognition of each individual constituent on an electron microscopic scale. This implies a direct coupling between light and transmission electron microscopy to be able to study each constituent in detail as well as the role of inclusions in developing the microstructure.

The experiments confirm that artificial aging leads to a harder and stronger but less tough material. This can be explained from the results of a TEM study carried out on an artificially aged single-bead ferritic weld metal (Ref. 21). This study shows that plastic deformation (6%) causes an increase in dislocation density and some dislocation cell formation. The net effect is a reduction in dislocation mobility, resulting in a harder but less tough material.

Subsequent annealing (30 minutes at 250°C, *i.e.,* 482°F) reveals pre-precipitation of interstitial atoms like N and C at dislocations within the ferrite grains. The result is a further shift of the transition curve to higher temperatures and a simultaneous decrease of the upper shelf energy (Refs. 7,8). This can be explained by stating that the precipitates cause an extra reduction in dislocation mobility, and obviously initiate microvoid coalescence (Ref. 14).

It is believed that similar processes are responsible for the differences upon artificial aging observed in the present study, although the role of Ti and B in removing N from solid solution, as observed elsewhere, is not clear at the moment (Refs. 22,23). TEM studies in combination with microanalytical techniques are needed to reveal further details.

Conclusion

In investigation described in this paper, the mechanical properties of two single-bead ferritic weld metals in the as-welded and artificially aged condition were compared with regard to the principal microstructural constituents, grain boundary ferrite, ferrite with aligned M-A-C and acicular ferrite. The investigation demonstrated that a higher proportion of acicular ferrite (at the expense of grain boundary ferrite) and a finer microstructure are not always beneficial to weld metal toughness. This can be attributed to a simultaneous increase in hardness and strength, offsetting the positive effects of more acicular ferrite and a smaller grain

Table 9—Proportion of the Principal Microstructural Constituents Along Crack Propagation Paths of Broken Charpy Specimens (As-Welded) in Comparison With the Bulk Proportion of These Constituents, Resulting in a Fracture Sensitivity Parameter (also see Fig. 6)

	Weld metal A			Weld metal B		
	Proportion of constituents, %			Proportion of constituents, %		
Constituents	Along crack patch	In bulk	Fracture sensitivity measure	Along crack patch	In bulk	Fracture sensitivity measure
GF	62.2	54.4	1.14	35.5	34.0	1.04
AC	25.1	18.2	1.38	27.7	16.3	1.70
AF	12.7	27.4	0.46	36.8	49.7	0.74

size. It is assumed that the higher hardness and strength properties are due to solid solution hardening of Mn, although transmission electron microscopy in combination with microanalytical techniques is needed to disclose further details.

The artificial aging process showed a varying influence on notch toughness, hardness, and strength, indicating differences between the principal microstructural constituents on a submicron scale. These differences were partly characterized by microhardness and crack propagation path measurements. The fracture sensitivity parameter indicated a different resistance to cleavage for each microstructural constituent. In terms of this condition it is possible to explain the notch toughness behavior of both weld metals with regard to their microstructure.

Acknowledgements

The authors are grateful to Ir. F.F. Westendorp and Mr. S.J. Verburg of Philips Welding Industries BV, Development Laboratories, Utrecht, The Netherlands, for many helpful discussions in the course of the investigation.

References

1. Munnig Schmidt-van der Burg, M. A., Hoekstra, S., and Den Ouden, G. 1984. *Microstructure and notch toughness of ferritic weld metal.* Philips Weld. Reporter, to be published.

2. Dolby, R. E. 1976. *Factors controlling weld toughness — the present position (Part 2, weld metals).* Welding Institute research report 14/1976/M.

3. Garland, J. G., and Kirkwood, P. R. 1975. Towards improved submerged arc weld metal (Part 1). *Met. Constr.* 7:275-283.

4. Garland, J. G., and Kirkwood, P. R. 1975. Towards improved submerged arc weld metal (Part 2). *Met. Constr.* 7:320-330.

5. Bonnet, C. 1980. Relation structure — résilience dans les soudures d'aciers doux et faiblement alliés brutes de solidification. *Soudage et Techniques Connexes* 34:209-230.

6. Harrison, P. L., Watson, M. N., and Farrar, R. A. 1981. How niobium influences SA mild steel weld metals (Part 2, Continuous cooling transformation (CCT) diagrams). *Weld. Met. Fab.* 49:161-169.

7. Cochrane, R. C., Terry, P., and Garland, J. G. 1976. Root-run toughness in multi-pass manual metal-arc welds (Part 1, The experimental approach). *Weld. Met. Fab.* 44:316-320.

8. Cochrane, R. C., Terry, P., and Garland, J. G. 1976. Root-run toughness in multi-pass manual metal-arc welds (Part 2, Results and discussion). *Weld, Met. Fab.* 44:439-448.

9. Otegui, J. L., Vega, R. A., and De Vedia, L. A. 1983. *Influence of dynamic strain aging on notch toughness of weld deposits.* IIW doc. II-A-581-83.

10. Mentink, H., Nühn, N. G. J., Verburg, S. J., and Westendorp, F. F. 1982. The development of consumables for offshore constructions. *Proc. int. conf. on offshore welded structures,* paper 32, pp. 1-8. London, England: The Welding Institute.

11. Abson, D. J., and Dolby, R. E. 1980. A scheme for the quantitative description of ferritic weld metal microstructures. *Welding Institute res. bull.* 21:100-103.

12. Evans, G. M. 1980. Effect of manganese on the microstructure and properties of all-weld-metal deposits. *Welding Journal* 59 (3):67-s to 75-s.

13. Farrar, R. A., and Watson, M. N. 1979. Effect of oxygen and manganese on submerged arc weld metal microstructures. *Met. Constr.* 11:285-286.

14. Broek, D. 1973. The role of inclusions in ductile fracture and fracture toughness. *Eng. Fract. Mech.* 5:55-66.

15. Ito, Y., Nakanishi, M., and Komizo, Y. 1982. Effects of oxygen on low carbon steel weld metal. *Met. Constr.* 14:472-478.

16. Cochrane, R. C. 1983. *Weld metal microstructures — A 'state-of-the-art' review.* IIW doc. II-A-580-83.

17. Taylor, L. G., and Farrar, R. A. 1975. Metallurgical aspects of the mechanical properties of submerged-arc weld metal. *Weld. Met. Fab.* 43:305-310.

18. Snyder, J. P., and Pense, A. W. 1982. The effects of titanium on submerged arc weld metal. *Welding Journal* 61(7):201-s to 211-s.

19. Tichelaar, G. W. 1983. Private communication.

20. Tweed, J. H., and Knott, J. F. 1983. Effect of reheating on microstructure and toughness of C-Mn weld metal. *Met. Sc.* 17:45-54.

21. Hoekstra, S., Munnig Schmidt-van der Burg, M. A., Mandziej, S., and Beyer, J. 1985. Effect of artificial strain aging on microstructure and mechanical properties of a single bead ferritic weld metal. To be published.

22. Tsuboi, J., and Terashima, H. 1981. *Review of strength and toughness of Ti and Ti-B microalloyed deposits.* IIW doc. II-A-526-81.

23. Mori, N., Homma, H., Okita, S., and Wakabayashi, M. 1981. *Mechanism of notch toughness improvement in Ti-B bearing weld metals.* IIW doc. IX-1196-81.